

Role of oxygen in laser-induced contamination at diamond-vacuum interfaces

Shreyas Parthasarathy¹, Maxime Joos,^{1,†} Lillian B. Hughes², Simon A. Meynell,¹ Taylor A. Morrison,¹ J.D. Risner-Jamtgaard³, David M. Weld,¹ Kunal Mukherjee,⁴ and Ania C. Bleszynski Jayich^{1,*}

¹Department of Physics, University of California, Santa Barbara, Santa Barbara, California 93106, USA

²Materials Department, University of California, Santa Barbara, Santa Barbara, California 93106, USA

³Stanford Nano Shared Facilities, Stanford University, Palo Alto, California 94305, USA

⁴Department of Materials Science and Engineering, Stanford University, Palo Alto, California 94305, USA

(Received 17 January 2024; revised 30 April 2024; accepted 8 July 2024; published 26 August 2024)

Many modern-day quantum science experiments rely on high-fidelity measurement of fluorescent signals emitted by the quantum system under study. A pernicious issue encountered when such experiments are conducted near a material interface in vacuum is “laser-induced contamination” (LIC): the gradual accretion of fluorescent contaminants on the surface where a laser is focused. Fluorescence from these contaminants can entirely drown out any signal from, e.g., optically probed color centers in the solid state. Crucially, while LIC appears often in this context, it has not been systematically studied. In this work, we probe the onset and growth rate of LIC for a diamond nitrogen-vacancy center experiment in vacuum, and we correlate the contamination-induced fluorescence intensities to micron-scale physical buildup of contaminant on the diamond surface. Drawing upon similar phenomena previously studied in the space optics community, we use photocatalyzed oxidation of contaminants as a mitigation strategy. We vary the residual oxygen pressure over 9 orders of magnitude and find that LIC growth is inhibited at near-atmospheric oxygen partial pressures, but the growth rate at lower oxygen pressure is nonmonotonic. Finally, we discuss a model for the observed dependence of LIC growth rate on oxygen content and propose methods to extend *in situ* mitigation of LIC to a wider range of operating pressures.

DOI: 10.1103/PhysRevApplied.22.024067

I. INTRODUCTION

Modern quantum science experiments often deploy a combination of vacuum environments, engineered material interfaces, and high-intensity light to achieve the degree of control and stability necessary for sensing, computation, and simulation. Vacuum plays the dual role of enabling cryogenic operation and mitigating harmful contaminants on material surfaces. These surfaces can limit qubit performance in a variety of ways: adsorbates on electrode surfaces generate electric field noise in ion traps [1–3]; charge traps in diamond limit stability of near-surface nitrogen-vacancy (N-V) centers [4,5], surface-related two-level systems limit superconducting qubit scalability and optomechanical resonator lifetimes [6–8]. While vacuum and low temperature alone sometimes ameliorate these issues and enable access to more desirable physical regimes, the introduction of high-intensity light can counterproductively generate surface contamination that shortens experimental lifespans. Here, we characterize this “laser-induced

contamination” (LIC)—the progressive accumulation of photochemically bonded, fluorescent matter at the site of a laser focused onto a surface—and its effect on visible wavelength color center experiments.

The N-V center in diamond is an optically addressable qubit known for its stability in ambient conditions. Despite the ostensible convenience of atmospheric conditions, vacuum and cryogenic operation of N-V centers provide many advantages, and in some cases is required. A variety of condensed-matter phenomena that are targets of sensing experiments only manifest at low temperatures [9,10]. Molecular targets (e.g., spin labels and biomolecules) can be susceptible to photodamage that is exacerbated at elevated temperatures or pressures [11,12]. Low-temperature operation also facilitates spin-photon entanglement [13], single-shot readout [14], and decreased spin relaxation and decoherence rates [15–17]. Additionally, improving spin coherence and charge stability of the shallow N-V used in nanoscale magnetometry experiments is an outstanding challenge that should benefit from the advanced level of surface characterization (e.g., LEED, XPS, NEXAFS) [18,19], treatment (e.g., annealing, surface cleaning) [20,21], and control (over, e.g., surface adsorbates

*Contact author: ania@physics.ucsb.edu

†Present address: Cailabs, 35000 Rennes, France.

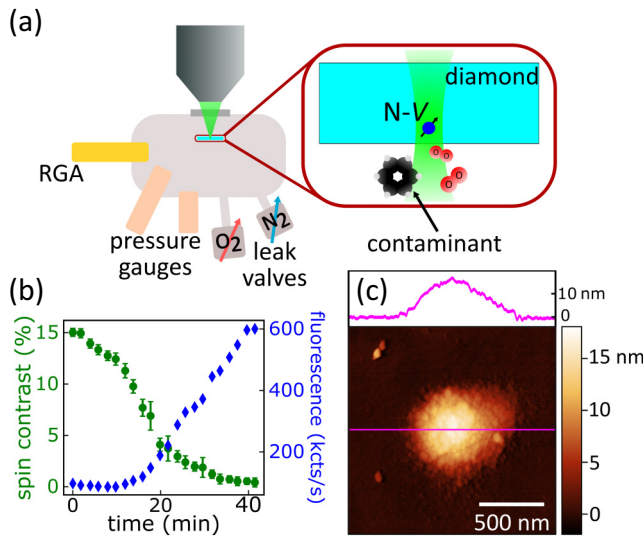


FIG. 1. (a) Schematic of vacuum chamber and experiment. A diamond sample with near-surface N-V centers resides inside a vacuum chamber outfitted with oxygen and nitrogen leak valves, a residual gas analyzer (RGA), and pressure gauges. An ambient microscope objective transmits 532-nm wavelength laser excitation and collects red fluorescence from both N-Vs and LIC. Inset shows a schematic view of the photochemistry underlying LIC: organic molecules, oxygen, and the diamond surface react under intense light immediately adjacent to the N-V under study. (b) Total fluorescence and N-V spin contrast plotted as a function of exposure time to laser illumination in vacuum. LIC-induced fluorescence eventually drowns out N-V fluorescence, reducing spin contrast to near zero. (c) Atomic force microscopy image and linecut (top) of laser-induced contamination grown on bulk diamond after 2 days of nearly continuous illumination.

[22–24]) that is accessible in an ultrahigh vacuum experiment. Fluorescent LIC is a persistent barrier to such progress; it has been observed in many vacuum N-V experiments, but to our knowledge is not yet discussed in the literature.

An example of LIC and its adverse impacts on N-V center experiments is depicted in Fig. 1. Here, LIC forms when a green (532-nm wavelength) laser is focused on a diamond surface held in the vacuum chamber depicted in Fig. 1(a). As LIC-induced background fluorescence accrues over time, it masks the spin-state-dependent fluorescence of the N-V center [Fig. 1(b)], ultimately limiting the duration of the experiment. Moreover, the physical accumulation of contaminants at the site of measurement [characterized using atomic force microscopy (AFM) in Fig. 1(c)] confounds study of other surface-related phenomena [20,25] and hinders vacuum experiments that require proximity to a target, such as scanning N-V magnetometry [26].

Although not actively studied in the solid-state qubit community, LIC has been extensively characterized in

the context of optics in space (primarily in the ultraviolet [27–31] and near-infrared [32–34] regimes). In the vacuum of space, LIC has the harmful capacity to reduce transmission through optical components and introduce wave-front error, threatening the commissioned lifetime of many satellite-based experiments where routine cleaning cannot occur (e.g., gravitational-wave observation [35,36], LIDAR-based surveys of planets and moons [37], atmospheric dynamics and aerosol measurement [38,39], etc., for a summary see Ref. [31]). This research community has identified hydrocarbon precursors for LIC and developed mitigation strategies tailored primarily to silica [30,39,40], often exploiting the well-established capacity for reactive oxygen species to degrade hydrocarbon contaminants [41,42].

In this work, we use the chamber depicted in Fig. 1 to systematically explore the conditions for LIC growth in an N-V center experiment. Inspired by progress on mitigating LIC in the aforementioned UV and IR space-based experiments, we expose a diamond surface to varying levels of oxygen and measure the resulting LIC growth under green laser illumination. Here, we report four central observations, which we believe pertain to all optically addressable solid-state systems (e.g., see the Supplemental Material [43] for LIC on silicon). First, we report significant LIC-induced fluorescence on diamond at room temperature for oxygen pressures ranging from 10^{-8} mbar to 10^{-2} mbar. Second, LIC fluorescence levels and physical volumes of LIC are correlated, in line with studies of LIC on other surfaces [39,40,44]. Third, the accumulation of LIC during N-V measurements is reproducibly controlled by residual oxygen concentration. This accumulation rate depends nonmonotonically on oxygen content: LIC growth is slow in a low oxygen environment, dramatically faster at intermediate oxygen pressures, and fully inhibited at near-atmospheric pressures (consistent with routine LIC-free operation in ambient conditions). Fourth, we demonstrate that illumination under oxygen-rich environments can be used as an *in situ* method to remove LIC in systems where contamination is unavoidable. We end by conjecturing possible mechanisms for LIC consistent with its ubiquity and observed kinetics and pathways for more efficient mitigation.

II. EXPERIMENTAL SETUP

An electronic grade (100) diamond substrate (Element Six) with an epitaxial layer of approximately 100 nm of CVD-grown, isotopically purified (99.998% ^{12}C) diamond was implanted with ^{14}N and oxygen-terminated using standard preparation procedures for shallow N-V center studies [43]. While LIC grows on the bulk diamond surface [Fig. 1(c)], we primarily used fabricated 670-nm diameter nanopillars to achieve more efficient excitation and fluorescence collection for N-Vs and LIC alike.

Measurements were performed in a stainless-steel vacuum chamber [Fig. 1(a)] with a water-dominated background pressure of 7×10^{-8} mbar, and sample temperature was 298 K. To control oxygen content, 99.999% molecular oxygen (Airgas OXR33A) was admitted into the chamber via an all-metal leak valve (Vacgen LVM) with electropolished stainless-steel lines (Superlok USA). Oxygen partial pressure was measured using a residual gas analyzer (SRS RGA200) at low pressures, and multiple pressure gauges at higher pressures.

All materials were chosen to conform to low outgassing standards (ASTM E595-77), as is typical practice for many vacuum experiments. A material inventory of the chamber and discussion of potential contaminant precursors is contained in Ref. [43].

III. CHARACTERIZING LIC FORMATION RATE

Our *in situ* probe of LIC was a home-built confocal microscope with 532-nm wavelength excitation and 652 – 1042 nm wavelength collection using a 0.7-NA objective. We focused 1.5 mW of laser power (approximately 430 kW/cm^2) continuously [43] on near-surface N-Vs in a series of nanopillars and tracked the buildup of fluorescence over time. Figure 2 compares characterization via confocal fluorescence measurements (under a lower

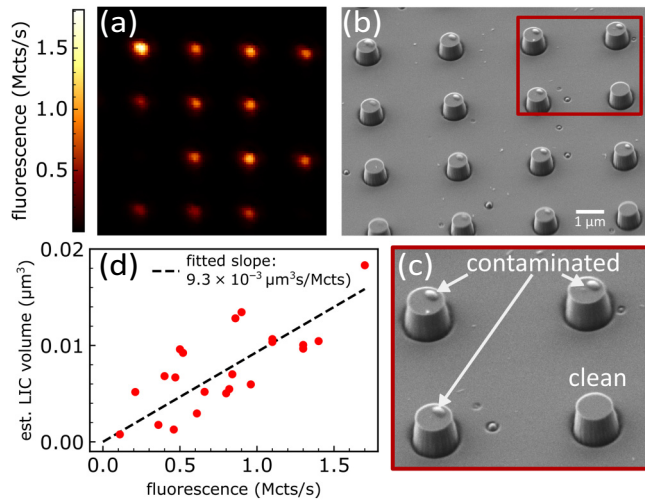


FIG. 2. (a) A confocal fluorescence image of LIC-contaminated nanopillars, taken at a low ($92 \mu\text{W}$) laser power to minimize additional contamination during the scan. Comparison to standard N-V fluorescence suggests counts are almost entirely (>95%) due to LIC. (b) SEM image of the pillars shown in (a) after removal of sample from chamber. Contamination is visible on pillar tops, likely forming in the region of highest field intensity (off center in this case [43]). (c) An enlarged region of the SEM image in (b). The bottom right pillar, which was not contaminated, is shown for comparison. (d) Scatter plot of estimated contaminant volume versus measured pillar fluorescence. A clear correlation is apparent.

excitation power of $92 \mu\text{W}$) and via *ex situ* scanning electron microscopy (SEM). Figure 2(a) is a fluorescence image of 16 nanopillars contaminated under varying illumination times (3–12 h) and oxygen pressures (10^{-4} to 10^{-2} mbar). After these exposures, LIC dominates the observed fluorescence. For comparison, typical N-V fluorescence rates for the excitation power used in Fig. 2(a) are approximately 50 kcts/s. We note the appearance of LIC-induced fluorescence on timescales that interfere with N-V experiments is not unique to this setup: the example depicted in Fig. 1(b) was produced with a different chamber and sample, yet shows similar growth dynamics.

Figure 2(b) shows the same pillars as Fig. 2(a), imaged via SEM after removal from the vacuum chamber. A bright mound of contamination is visible on each nanopillar, from which contaminant volume can be estimated. Figure 2(c) is an enlarged region of Fig. 2(b). Figure 2(d) is a scatter plot of measured fluorescence and LIC volume estimated from the SEM image for 22 different pillars. The plot reveals a correlation between fluorescence intensity and the physical size of deposits. From this trend, we extract an LIC volume-to-fluorescence ratio for our setup of approximately $9 \times 10^{-3} \mu\text{m}^3 \text{ s/Mcts}$ under $92 \mu\text{W}$ of excitation, which corresponds to approximately $6 \times 10^{-4} \mu\text{m}^3 \text{ s/Mcts}$ at the 1.5 mW used in Fig. 3. With this calibration, we use LIC fluorescence intensity growth as a proxy for volume growth (see Fig. 3), a technique also deployed by the broader community [29,39,44].

IV. ROLE OF OXYGEN IN CONTAMINATION RATE

We next examine the dependence of LIC formation on molecular oxygen partial pressure. Figure 3(a) plots the increase in fluorescence after 200 min of illumination at constant 1.5 mW as a function of measured partial pressure P_{O_2} . A control experiment using nitrogen gas confirms that the effect is due to only total oxygen content, rather than pressure-related effects alone [43]. We identify three different LIC formation regimes.

Regime I: For $P_{O_2} \lesssim 5 \times 10^{-3}$ mbar, the LIC growth rate increases as P_{O_2} increases. Figure 3(b) shows four representative curves of fluorescence as a function of illumination time. The onset of LIC growth is immediate, but the rate increases with increasing P_{O_2} , until growth is fastest at $P_{O_2} \sim 4.6 \times 10^{-3}$ mbar.

Regime II: A distinctly different regime occurs for approximately $5 \times 10^{-3} < P_{O_2} < 2$ mbar. Figure 3(c) plots representative fluorescence growth curves in this regime. Once contamination starts, the rate of LIC growth is similar to the peak growth rate observed in regime I. However, onset of contamination is delayed, with a delay time that increases as P_{O_2} increases. In Fig. 3(a), this effect manifests as an abrupt decrease in the average level of fluorescence after 200 min.

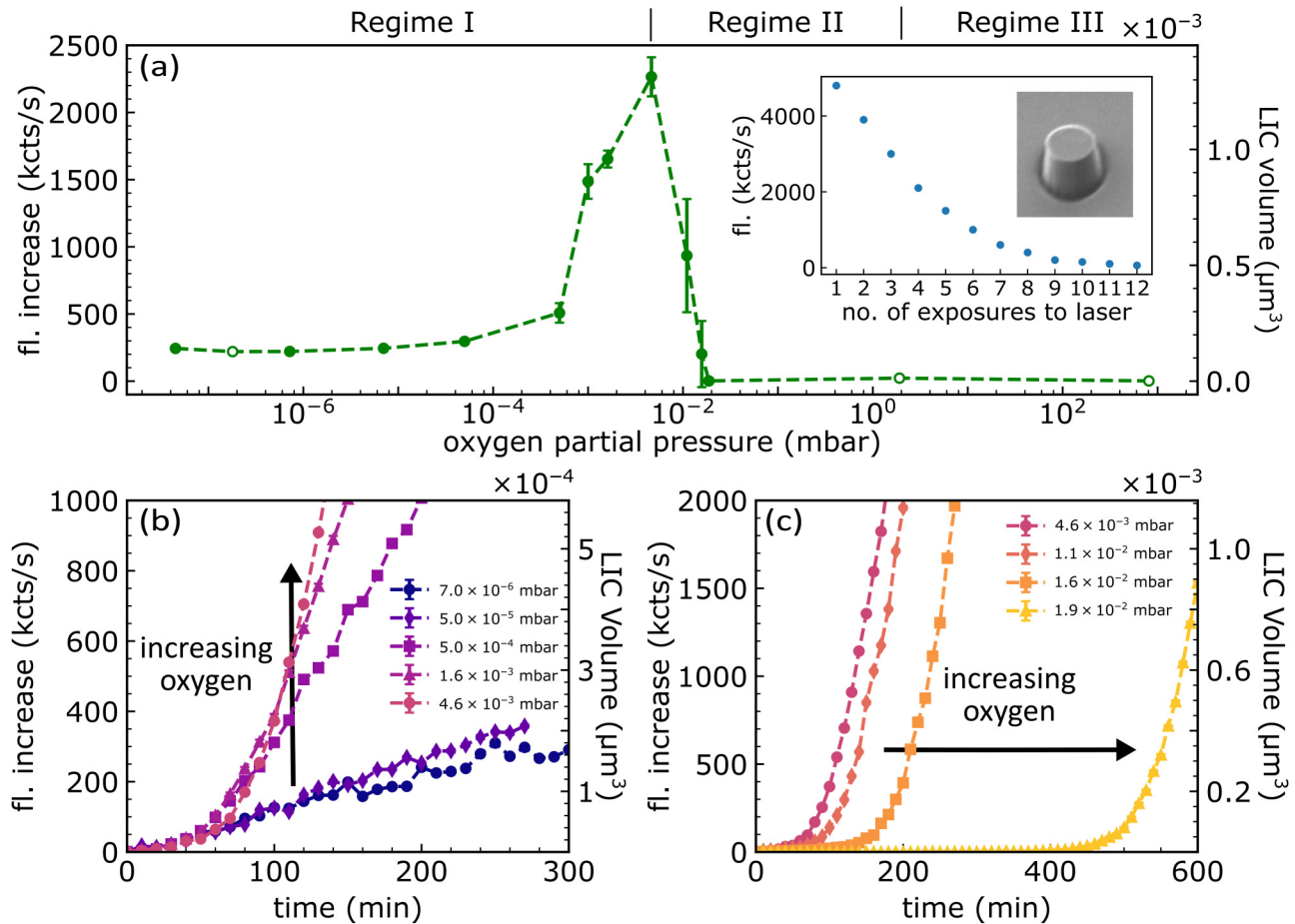


FIG. 3. (a) Average change in fluorescence (fl.) and calculated LIC volume (using the correlation from Fig. 2) after 200 min of laser illumination at various oxygen partial pressures. Each filled marker is the mean fluorescence increase averaged over multiple nanopillars contaminated at the same partial pressure. Error bars are 68% confidence intervals. Unfilled markers are derived from observations of single nanopillars. Inset shows degradation of LIC under successive light exposures in an oxygen-rich (regime III) environment. An SEM image of the treated pillar shows a top surface free of detectable contaminants, implying that the laser exposure physically removes LIC. (b) Representative LIC growth curves for regime I. Increasing oxygen pressure increases the growth rate. Error bars are smaller than the size of data points. Details of how fluorescence was sampled, averaged, and compared are given within the Supplemental Material [43]. (c) Representative LIC-induced fluorescence growth curves for regime II. Increasing oxygen delays the onset of LIC growth.

Regime III: Finally, LIC ceases to form for $P_{O_2} > 2$ mbar. In this regime, LIC is fully inhibited. Additionally, exposing existing LIC deposits to light removes their associated fluorescence, and subsequent SEM imaging confirms physical removal of contaminants [see inset in Fig. 3(a)].

V. MODEL FOR CONTAMINATION

Our results provide valuable insight into the formation mechanisms of LIC. The strongly nonmonotonic dependence of LIC growth rate on oxygen content suggests photoactivated molecular oxygen must participate in competing growth and etch processes on the diamond surface. At high oxygen content, etching of LIC

is consistent with photocatalyzed oxidation of an organic or graphitic contaminant. Carbon-based composition comports with reported spectroscopy of macroscopic LIC in other systems [30] and our Auger-electron spectroscopy measurements [43]. The threshold pressure for oxidation is consistent with results for UV-catalyzed LIC on vacuum windows [39] suggesting inhibition occurs via gaseous oxidation independent of substrate. At lower oxygen pressures, oxidation is not the dominant process. Many other processes involving a variety of reactants (e.g., oxygen, organic LIC precursors, water, dangling bonds on the diamond surface, etc.) are plausible.

Here we outline one model of competing reactions involving oxygen, hydrocarbons, and surfaces [42,45,46], and show that our model can qualitatively reproduce the

behavior depicted in Fig. 3. Rate equations, numerics, and potential variants of the model can be found in Ref. [43].

Our model supposes the LIC process consists of three reactions with first-order kinetics, all photocatalyzed:

(A) A surface-limited growth reaction at the vacuum-diamond interface between adsorbed oxygen and adsorbed LIC precursors (rate-limiting at early times and/or low P_{O_2}), obeying Langmuir-Hinschelwood kinetics [47].

(B) An oxygen-independent reaction at the vacuum-LIC interface where gaseous LIC precursors attach to LIC deposits directly. This reaction dominates once seed contaminants have sufficiently large surface area.

(C) An oxidation reaction that consists of photoactivated oxygen decomposing LIC.

We now discuss how this model can qualitatively produce the regimes in Fig. 3:

Regime I: Dynamics in Fig. 3(b) are primarily driven by reaction A: as P_{O_2} is increased, more oxygen adsorbs onto the diamond surface and encourages LIC growth via reaction A. At late times, all surface-mediated sites where reaction A can proceed are depleted. Reaction B is independent of adsorbates and thus dominates. Fast, linear growth occurs [see late times in Fig. 3(b), $P_{O_2} = 1.6 \times 10^{-3}$ mbar or Fig. 3(c)].

Regime II: For $P_{O_2} \gtrsim 5 \times 10^{-3}$ mbar, two effects subdue the initial growth rate. First, adsorbed oxygen displaces adsorbed LIC precursors, which impedes growth via reaction A. Second, gaseous oxygen starts etching existing LIC (via reaction C), slowing net growth. Still, when enough LIC eventually forms at late times, reaction B dominates and the same maximal growth rate is observed. Rather than complete elimination of LIC, inhibition first manifests as the delayed onset seen in Fig. 3(c).

Regime III: Finally, when P_{O_2} is high enough, reaction C dominates and LIC ceases to form.

VI. MITIGATION METHODS

A. Prevention

Our measurements indicate that standard vacuum practices do not necessarily avoid LIC. Hence, in addition to undergoing species-insensitive outgassing tests, vacuum materials should be screened for chemical composition and/or compatibility in an LIC test chamber (as is already done in experiments with particularly stringent reliability requirements such as LISA, LIGO, etc. [27,37,48,49]). To theoretically predict which materials are prone to producing LIC, direct chemical analysis of composition and formation is necessary. While the small volumes in this experiment are not resolvable via many *in situ* characterization methods, additional analysis of LIC absorption and fluorescence (e.g., spectral shifts during growth or kinetics

as a function of wavelength) could further elucidate reaction mechanisms.

B. Oxidation

For N-V experiments, venting with oxygen and removing LIC with the same laser used for spin readout is considerably less invasive than sample removal and *ex situ* cleaning. This study suggests boosting the reactivity of residual oxygen in vacuum is key to inhibition of LIC at lower pressures. To that end, introducing atomic or ozone-based oxygen treatments [19] may increase the effective etch rate by many orders of magnitude [32]. Alternatively, ultrahigh vacuum chambers may incorporate load locks for the explicit purpose of periodic cleaning with oxygen and light without partial venting.

C. Substrate control

A parallel substrate-specific route towards inhibition requires more detailed study of LIC growth rate as a function of surface preparation. Surface roughness, susceptibility to charging, baking to remove adsorbates, changing surface termination, and protective capping layers likely affect the kinetics of LIC formation (and in some cases, have already been shown to do so. See the Supplemental Material [43] for preliminary evidence that conductivity of a silicon substrate may affect LIC formation and a brief review of LIC mitigation in other contexts [31,39]). Finally, we note that while LIC formation reactions are photocatalyzed (and thus temperature is not a primary activation mechanism), a small Arrhenius coefficient may still have a large and beneficial effect when anticipating the likelihood of LIC for cryogenic experiments.

VII. CONCLUSION

In conclusion, we have shown the phenomenon of laser-induced fluorescence often seen in vacuum quantum science experiments is due to the photocatalyzed accretion of physical material, a process also observed in space optics experiments. The contamination growth rate varies widely and nonmonotonically with oxygen concentration; oxygen can either encourage or inhibit contamination due to multiple competing processes, but is an effective mitigant at high enough pressures. We propose one set of competing reactions involving the diamond surface, contaminants, adsorbed oxygen, and gaseous oxygen that qualitatively reproduces the behavior we observe.

As lasers and vacuum become an indispensable element in increasingly complicated quantum science experiments, deep technical understanding of failure mechanisms is essential. Our approach suggests several pathways towards elimination of one particularly destructive mechanism. Moreover, light-induced surface deterioration in diamond, especially in vacuum, is known to limit shallow N-V spin

coherence and charge stability. While these changes are not well understood, we suspect the origin of these effects may be closely related to early-time LIC-related processes. Controlled experiments probing this chemistry will therefore be critical to enabling both LIC-free operation in vacuum and tackling these more subtle, yet fundamental limitations to defect centers in the solid state.

ACKNOWLEDGMENTS

We gratefully acknowledge support of the U.S. Department of Energy BES Grant No. DE-SC0019241. We acknowledge the use of shared facilities of the UCSB Quantum Foundry through Q-AMASE-i program (NSF DMR-1906325), the UCSB MRSEC (NSF DMR 1720256), and the Quantum Structures Facility within the UCSB California NanoSystems Institute. D.M.W. and A.B.J. acknowledge support from the NSF QLCI program through Grant No. OMA-2016245. A.B.J. acknowledges support from Cooperative Research on Quantum Technology (2022M3K4A1094777) through the National Research Foundation of Korea (NRF) funded by the Korean Government [Ministry of Science and ICT (MSIT)]. Portions of this work were performed in the UCSB Nanofabrication Facility, an open access laboratory, and at the Stanford Nano Shared Facilities (SNSF), supported by the National Science Foundation under award ECCS-2026822. S.P. acknowledges support from the Department of Defense (DoD) through the National Defense Science and Engineering Graduate (NDSEG) Fellowship Program. L.B.H. acknowledges support from the NSF Graduate Research Fellowship Program (DGE 2139319) and the UCSB Quantum Foundry. S.A.M. acknowledges support from the UCSB Quantum Foundry. We thank Rob Knowles and Kurt Olsson for helpful discussions, and Pooja Reddy and Rachel Schoeppner for preliminary experiments.

- [1] J. Chiaverini and J. M. Sage, Insensitivity of the rate of ion motional heating to trap-electrode material over a large temperature range, *Phys. Rev. A* **89**, 012318 (2014).
- [2] E. Kim, A. Safavi-Naini, D. A. Hite, K. S. McKay, D. P. Pappas, P. F. Weck, and H. R. Sadeghpour, Electric-field noise from carbon-adatom diffusion on a Au(110) surface: First-principles calculations and experiments, *Phys. Rev. A* **95**, 033407 (2017).
- [3] K. R. Brown, J. Chiaverini, J. M. Sage, and H. Häffner, Materials challenges for trapped-ion quantum computers, *Nat. Rev. Mater.* **6**, 892 (2021).
- [4] D. Bluvstein, Z. Zhang, and A. C. B. Jayich, Identifying and mitigating charge instabilities in shallow diamond nitrogen-vacancy centers, *Phys. Rev. Lett.* **122**, 076101 (2019).
- [5] Y. Chu, N. De Leon, B. Shields, B. Hausmann, R. Evans, E. Togan, M. J. Burek, M. Markham, A. Stacey, A. Zibrov, A. Yacoby, D. Twitchen, M. Loncar, H. Park, P. Maletinsky,

- and M. Lukin, Coherent optical transitions in implanted nitrogen vacancy centers, *Nano Lett.* **14**, 1982 (2014).
- [6] J. Gao, M. Daal, J. M. Martinis, A. Vayonakis, J. Zmuidzinas, B. Sadoulet, B. A. Mazin, P. K. Day, and H. G. Leduc, A semiempirical model for two-level system noise in superconducting microresonators, *Appl. Phys. Lett.* **92**, 212504 (2008).
- [7] K. D. Crowley *et al.*, Disentangling losses in tantalum superconducting circuits, *Phys. Rev. X* **13**, 041005 (2023).
- [8] G. S. MacCabe, H. Ren, J. Luo, J. D. Cohen, H. Zhou, A. Sipahigil, M. Mirhosseini, and O. Painter, Nano-acoustic resonator with ultralong phonon lifetime, *Science* **370**, 840 (2020).
- [9] A. Jenkins, S. Baumann, H. Zhou, S. A. Meynell, Y. Daipeng, K. Watanabe, T. Taniguchi, A. Lucas, A. F. Young, and A. C. Bleszynski Jayich, Imaging the breakdown of ohmic transport in graphene, *Phys. Rev. Lett.* **129**, 087701 (2022).
- [10] M. Borst, P. H. Vree, A. Lowther, A. Teepe, S. Kurdi, I. Bertelli, B. G. Simon, Y. M. Blanter, and T. Van Der Sar, Observation and control of hybrid spin-wave–Meissner-current transport modes, *Science* **382**, 430 (2023).
- [11] D. Pinto, D. Paone, B. Kern, T. Dierker, R. Wieczorek, A. Singha, D. Dasari, A. Finkler, W. Harneit, J. Wrachtrup, and K. Kern, Readout and control of an endofullerene electronic spin, *Nat. Commun.* **11**, 6405 (2020).
- [12] M. Eckardt, R. Wieczorek, and W. Harneit, Stability of C₆₀ and N@C₆₀ under thermal and optical exposure, *Carbon* **95**, 601 (2015).
- [13] H. Bernien, B. Hensen, W. Pfaff, G. Koolstra, M. S. Blok, L. Robledo, T. H. Taminiau, M. Markham, D. J. Twitchen, L. Childress, and R. Hanson, Heralded entanglement between solid-state qubits separated by three metres, *Nature* **497**, 86 (2013).
- [14] D. M. Irber, F. Poggiali, F. Kong, M. Kieschnick, T. Lühmann, D. Kwiatkowski, J. Meijer, J. Du, F. Shi, and F. Reinhard, Robust all-optical single-shot readout of nitrogen-vacancy centers in diamond, *Nat. Commun.* **12**, 532 (2021).
- [15] S. Takahashi, R. Hanson, J. van Tol, M. S. Sherwin, and D. D. Awschalom, Quenching spin decoherence in diamond through spin bath polarization, *Phys. Rev. Lett.* **101**, 047601 (2008).
- [16] A. Jarmola, V. M. Acosta, K. Jensen, S. Chemerisov, and D. Budker, Temperature- and magnetic-field-dependent longitudinal spin relaxation in nitrogen-vacancy ensembles in diamond, *Phys. Rev. Lett.* **108**, 197601 (2012).
- [17] N. Bar-Gill, L. Pham, A. Jarmola, D. Budker, and R. Walsworth, Solid-state electronic spin coherence time approaching one second, *Nat. Commun.* **4**, 1743 (2013).
- [18] N. Dontschuk, L. Rodgers, J. Chou, D. Evans, K. M. O’Donnell, H. Johnson, A. Tadich, A. Schenk, A. Gali, N. De Leon, and A. Stacey, X-ray quantification of oxygen groups on diamond surfaces for quantum applications, *Mater. Quantum Technol.* **3**, 045901 (2023).
- [19] S. Kawai *et al.*, Nitrogen-terminated diamond surface for nanoscale NMR by shallow nitrogen-vacancy centers, *J. Phys. Chem. C* **123**, 3594 (2019).
- [20] S. Sangtawesin, B. L. Dwyer, S. Srinivasan, J. J. Allred, L. V. H. Rodgers, K. De Greve, A. Stacey, N. Dontschuk,

- K. M. O'Donnell, D. Hu, D. A. Evans, C. Jaye, D. A. Fischer, M. L. Markham, D. J. Twitchen, H. Park, M. D. Lukin, and N. P. de Leon, Origins of diamond surface noise probed by correlating single-spin measurements with surface spectroscopy, *Phys. Rev. X* **9**, 031052 (2019).
- [21] M. Kim, H. J. Mamin, M. H. Sherwood, C. T. Rettner, J. Frommer, and D. Rugar, Effect of oxygen plasma and thermal oxidation on shallow nitrogen-vacancy centers in diamond, *Appl. Phys. Lett.* **105**, 042406 (2014).
- [22] J. N. Neethirajan, T. Hache, D. Paone, D. Pinto, A. Denisenko, R. Stöhr, P. Udvaryhelyi, A. Pershin, A. Gali, J. Wrachtrup, K. Kern, and A. Singha, Controlled surface modification to revive shallow NV⁻ centers, *Nano Lett.* **23**, 2563 (2023).
- [23] M. V. Hauf, B. Grotz, B. Naydenov, M. Dankerl, S. Pezzagna, J. Meijer, F. Jelezko, J. Wrachtrup, M. Stutzmann, F. Reinhard, and J. A. Garrido, Chemical control of the charge state of nitrogen-vacancy centers in diamond, *Phys. Rev. B* **83**, 081304(R) (2011).
- [24] U. Zvi, D. R. Candido, A. Weiss, A. R. Jones, L. Chen, I. Golovina, X. Yu, S. Wang, D. V. Talapin, M. E. Flatté, A. P. Esser-Kahn, and P. C. Maurer, Engineering spin coherence in core-shell diamond nanocrystals, [arXiv:2305.03075](https://arxiv.org/abs/2305.03075).
- [25] M. Kim, H. J. Mamin, M. H. Sherwood, K. Ohno, D. D. Awschalom, and D. Rugar, Decoherence of near-surface nitrogen-vacancy centers due to electric field noise, *Phys. Rev. Lett.* **115**, 087602 (2015).
- [26] P. Maletinsky, S. Hong, M. S. Grinolds, B. Hausmann, M. D. Lukin, R. L. Walsworth, M. Loncar, and A. Yacoby, A robust scanning diamond sensor for nanoscale imaging with single nitrogen-vacancy centres, *Nat. Nanotechnol.* **7**, 320 (2012).
- [27] J. G. Daly, *Proc. SPIE 9573, Optomechanical Engineering 2015* (San Diego, California, United States, 2015), p. 95730C.
- [28] F. R. Wagner, G. Gebrayel El Readdy, D. Faye, and J.-Y. Natoli, Laser induced deposits in contaminated vacuum environment: Optical properties and lateral growth, *Opt. Laser Technol.* **122**, 105889 (2020).
- [29] G. Gebrayel El Readdy, F. R. Wagner, D. Faye, and J.-Y. Natoli, Study of the first stages of laser-induced contamination, *Opt. Eng.* **57**, 1 (2018).
- [30] A. P. Tighe, F. Pettazzi, J. Alves, D. Wernham, W. Riede, H. Schroeder, P. Allenspacher, and H. Kheyrandish, *Proc. SPIE 7132, Laser-Induced Damage in Optical Materials: 2008* (Boulder, CO, 2008), p. 71321L.
- [31] W. Riede, H. Schroeder, G. Bataviciute, D. Wernham, A. Tighe, F. Pettazzi, and J. Alves, *Proc. SPIE 8190, Laser-Induced Damage in Optical Materials: 2011* (Boulder, Colorado, 2011), p. 81901E.
- [32] N. Bartels, P. Allenspacher, W. Riede, H. Schröder, and D. Wernham, in *Laser-induced Damage in Optical Materials 2019*, edited by V. E. Gruzdev, C. W. Carr, D. Ristau, and C. S. Menoni (SPIE, Broomfield (Boulder area), United States, 2019), p. 7.
- [33] X. Ling, Y. Zhao, D. Li, S. Li, M. Zhou, J. Shao, and Z. Fan, Impact of organic contamination on the laser-induced damage in vacuum, *Appl. Surf. Sci.* **255**, 9255 (2009).
- [34] F. E. Hovis, B. A. Shepherd, C. T. Radcliffe, A. L. Bailey, and W. T. Boswell, *Proc. SPIE 2114, Laser-Induced Damage in Optical Materials: 1993* (Boulder, CO, 1994), p. 145.
- [35] N. Bartels, M. Vogel, W. Riede, C. Dahl, K.-C. Voss, A. Ciapponi, R. Martins, and L. Mondin, Laser-induced molecular contamination de-risking activity for the Laser Interferometer Space Antenna, *Appl. Opt.* **62**, 7091 (2023).
- [36] M. H. Phelps, K. E. Gushwa, and C. I. Torrie, *Proc. SPIE 8885, Laser-Induced Damage in Optical Materials: 2013* (Boulder, Colorado, USA, 2013), p. 88852E.
- [37] P. Chen, R. Hedgeland, L. Ramsey, R. Rivera, and K. Houston, *Proc. SPIE 6291, Optical Systems Degradation, Contamination, and Stray Light: Effects, Measurements, and Control II* (San Diego, California, USA, 2006), p. 629104.
- [38] F. E. Hovis, *Proc. SPIE 6100, Solid State Lasers XV: Technology and Devices* (San Jose, CA, 2006), p. 61001X.
- [39] D. Wernham, J. Alves, F. Pettazzi, and A. P. Tighe, *Proc. SPIE 9952, Systems Contamination: Prediction, Control, and Performance 2016* (Boulder, Colorado, 2010), p. 78421E.
- [40] M. Hippler, P. Wagner, H. Schroeder, and W. Riede, *Laser-Induced Contamination of Space Borne Laser Systems: Impact of Organic Contamination and Mitigation by Oxygen* (San Diego, California, United States, 2016), p. 99520N.
- [41] J. M. Anglada, M. Martins-Costa, J. S. Francisco, and M. F. Ruiz-López, Interconnection of reactive oxygen species chemistry across the interfaces of atmospheric, environmental, and biological processes, *Acc. Chem. Res.* **48**, 575 (2015).
- [42] V. A. Bhanu and K. Kishore, Role of oxygen in polymerization reactions, *Chem. Rev.* **91**, 99 (1991).
- [43] See Supplemental Material at <http://link.aps.org/supplemental/10.1103/PhysRevApplied.22.024067> for additional experimental details, LIC measurements in other contexts, discussion of physical characteristics of LIC, and model details and modifications, which also includes Refs. [50–57].
- [44] H. Schröder, S. Becker, Y. Lien, W. Riede, and D. Wernham, *Proc. SPIE 6720, Laser-Induced Damage in Optical Materials: 2007* (Boulder, CO, 2007), p. 67200O.
- [45] T. B. Stewart, G. S. Arnold, D. F. Hall, and H. D. Marten, Absolute rates of vacuum-ultraviolet photochemical deposition of organic films, *J. Phys. Chem.* **93**, 2393 (1989).
- [46] G. Delzenne, W. Dewinter, S. Toppet, and G. Smets, Photo-sensitized polymerization of acrylic monomers. II. Kinetics of polymerization in the presence of oxygen, *J. Polym. Sci. A: Gen. Pap.* **2**, 1069 (1964).
- [47] P. Atkins, J. D. Paula, and J. Keeler, *Physical Chemistry* (Oxford University Press, New York, NY, 2022), 12th ed.
- [48] D. Li, D. Coyne, and J. Camp, Optical contamination screening of materials with a high-finesse Fabry-Perot cavity resonated continuously at 106-μm wavelength in vacuum, *Appl. Opt.* **38**, 5378 (1999).
- [49] H. Schröder, P. Wagner, D. Kokkinos, W. Riede, and A. Tighe, *Proc. SPIE 8885, Laser-Induced Damage in Optical Materials: 2013* (Boulder, Colorado, USA, 2013), p. 88850R.
- [50] H. J. Mathieu, in *Surface Analysis: The Principal Techniques*, edited by J. C. Vickerman (John Wiley & Sons, Ltd, Chichester, West Sussex, UK, 1997), p. 99.

- [51] G. C. Smith, in *Updates in Applied Physics and Electrical Technology*, edited by P. Dobson (Plenum Press, New York, 1994).
- [52] K. K. Rohatgi-Mukherjee, *Fundamentals of Photochemistry* (Wiley Eastern Limited, Delhi, India, 1986), revised ed.
- [53] Y. Tatsukami, T. Takahashi, and H. Yoshioka, Reaction mechanism of oxygen-initiated ethylene polymerization at high pressure, *Die Makromolekulare Chemie* **181**, 1107 (1980).
- [54] R. L. Hansen, Kinetics and mechanism of the trialkylboron-catalyzed polymerization of methyl methacrylate in the presence of oxygen, *J. Polym. Sci. A: Gen. Pap.* **2**, 4215 (1964).
- [55] J. Asua, *Polymer Reaction Engineering* (John Wiley & Sons, Oxford, UK, 2008).
- [56] W. E. Farneth, F. Ohuchi, R. H. Staley, U. Chowdhry, and A. W. Sleight, Mechanism of partial oxidation of methanol over molybdenum (VI) oxide as studied by temperature-programmed desorption, *J. Phys. Chem.* **89**, 2493 (1985).
- [57] R. E. Thomas, R. A. Rudder, and R. J. Markunas, Thermal desorption from hydrogenated and oxygenated diamond (100) surfaces, *J. Vac. Sci. Technol. A: Vac., Surf., Films* **10**, 2451 (1992).
- [58] L. B. Hughes, Z. Zhang, C. Jin, S. A. Meynell, B. Ye, W. Wu, Z. Wang, E. J. Davis, T. E. Mates, N. Y. Yao, K. Mukherjee, and A. C. Bleszynski Jayich, Two-dimensional spin systems in PECVD-grown diamond with tunable density and long coherence for enhanced quantum sensing and simulation, *APL Mater.* **11**, 021101 (2023).